

## Development of Ni - Nano Al<sub>2</sub>O<sub>3</sub> coated AISI1018 mild steel composites via pulse electro deposition and investigation of its wear and corrosion behavior

S. Shanmugam<sup>a,\*</sup>, S. Mahalingam<sup>b</sup> and A. Ranjithkumar<sup>c</sup>

<sup>a</sup>Dept. of Mechanical Engineering, AVS College of Technology, Salem-636106, Tamil Nadu, India

<sup>b,c</sup>Dept. of Mechanical Engineering, SONA College of Technology, Salem-636005, Tamil Nadu, India

Scientists attempting to create a variety of tiny industrial components are very interested in AISI1018 mild steel due to its improved elasticity, low carbon content, and cost-effectiveness. For different technical and structural requirements, such as metal panels, engine components, highly pressurized chemical pipelines, machinery parts, and vehicle bonnets, the current research employs mild steel as a cornerstone matrix to generate Ni - Nano Al<sub>2</sub>O<sub>3</sub> Coated AISI1018 Mild Steel Composites. In order to determine the ideal Ni - Nano Al<sub>2</sub>O<sub>3</sub> wt. % that displays the best corrosion, mechanical, and surface morphology behavior, a Ni - Nano Al<sub>2</sub>O<sub>3</sub> coating on mild steel with variable Al<sub>2</sub>O<sub>3</sub> was applied using a reverse pulse electro deposition approach. According to research observations, increasing the proportion of Al<sub>2</sub>O<sub>3</sub> on the exterior of mild steel has a considerable positive impact on mechanical behavior, abrasion resistance, and chemical resistance. Hardness of the HMSAL6 samples plated with 3% Al<sub>2</sub>O<sub>3</sub> was 296 HV, which is almost 25% higher than the hardness of the plain samples. Similar studies on corrosion and wear have shown that a 25-40% improvement in corrosion and wear characteristics may be achieved by progressively increasing the amount of Ni-Al<sub>2</sub>O<sub>3</sub>. Through the use of field emission scanning electron microscopy, the efficiency of the reverse pulse electro deposition technique was also examined. It was discovered from the images that the surface of the mild steel is evenly distributed with the included Ni - Nano Al<sub>2</sub>O<sub>3</sub>.

**Keywords:** AISI1018 Mild Steel, Nano Al<sub>2</sub>O<sub>3</sub>, Nickel, Pulse electro deposition approach, Corrosion behavior, Mechanical behavior, Structural applications.

### Introduction

Mild steel is famous for having a low carbon footprint between 0.05% and 0.25%, which is substantially lower than high carbon steel (2.5%). Due to its special qualities, such as machinability, weldability, ductility, affordability, and electromagnetic tendency, mild steel attracts a lot of interest from all major firms in the industry for a diverse range of structural purposes [1-3]. The combo of abrasion and wear resistance offered by nickel plating is exceptional. It can enhance elegance, shine, and luminosity. The way it is written leads one to infer that nickel and titanium coatings are “paints”, which is not true [4, 5]. Aluminum Oxide may be employed in high thermal working situations and doesn't conflict with contaminants. It has outstanding thermal conductivity, friction, cavitations, particle erosion, oxidation, and abrasive wear. Additionally, it has a high service temperature with a 1649°C thermal insulator [6].

The presence of oxidant, and ions will cause mild steel, which is highly reactive, to quickly transform back into iron oxide (rust). Steel needs to be sufficiently

shielded from the weather in order to maintain and surpass its serviceability since it is ready to deteriorate when exposed to the environment outside [7-9]. Metals, ceramics, alloys, metallic oxides, and composites may all be deposited using the flexible and economical technique known as Pulse Electro - Deposition (PED). By appropriately adjusting the depositing capacity, it offers the special benefits of allowing control over coating density and chemical structure [10, 11]. Juglone derived from walnut green husk was studied by Shahmoradi et al. [12] for its ability to prevent rusting in mild steel samples subjected to an acid environment (1 M HCl). According to their findings, using more green chemical treatment (GCI) increased the effectiveness of the utilized inhibitor, reaching 95% in the existence of 800 ppm after an 8-hour soaking. Generally reverse pulse coating possess following benefits over normal pulse coatings such as lower process limitations, Better control of metal content in bath, Lower requirements of additives, Plating time or process time reduces.

For the preservation of mild steel erosion in acid solution media, Weiwei et al. [13] developed efficient and sustainable reducing agents that used a natural polysaccharide mixture inhibitor composed of chondroitin sulphate derived from pig cartilage (CS-PC) and sodium alginate (SA). He discovered that CS-SA acts as an

\*Corresponding author:  
Tel : +91-9789569056  
E-mail: shanmugam.subhu@gmail.com

efficient and environmentally green corrosion inhibitor in Hydrochloride media. According to Emanuel et al. [14] m-pentadecylphenol was synthesized from cashew nut shell liquid (CNSL), a cheap and sustainable resource, and is an efficient and environmentally reliable corrosion inhibitor for acid conditions.

Using diverse tungsten electrode materials, including copper tungsten and silver tungsten, Jahan et al. [15] experimented with micro-EDM of tungsten carbide and discovered that silver tungsten electrodes are capable of creating smooth, shining surfaces with a small degree of surface imperfections. Parallel to this, Chandrasatheesh et al. [16] created a microbially synthetic covering using Ag-TiO<sub>2</sub> (AgT) sol and cardanol epoxy (CE), coated mild steel (MS) substrates with it, and then examined its effectiveness at resisting corrosion. According to their findings, the combination of GAgT and CE matrix increased hydrophobicity while lowering surface free energy, which reduced the interfacial contacts between bacteria and MS substrates.

Using a variety of interfacial engineering technologies, such as electro pulsing aided ultra - sonic surface rolling process [17], chromium ion implantation [18], friction stir processing (FSP) [19], laser surface modification [20, 21] and thermal diffusion [22], there is an enhanced desire to enhance the wear and corrosion resistances of marine and structural products. However, this approach is expensive to deploy for large-scale commercial items and has substantial inventory expenses. Identical to that, nickel co-deposition coverings are frequently applied to metallic platforms' to improve their hardness, damage tolerance, abrasion, brilliance, and elevated heat chemical stability [23-28]. To improve the efficacy of protection against corrosion, nano materials are thought of as fillers for anti-corrosion coating materials [29]. The EIS approach has been widely employed in latest days to examine the corrosion performance and behavior of surface coatings [30]. It has been shown to be a potent instrument that can also produce meaningful results [31]. Dae-Seon Lee et al. [32] reported that inclusion of nano fillers into the metal matrix reported the maximum sintering behaviour along with the enhanced mechanical properties. Similarly Subhas Chandra Mondal et al. [33] showed that Multi Wall Carbon Nanotube-coated copper electrodes outperform pure copper electrodes.

Despite the fact that many studies have been published in the literature that combined pulse electro deposition with AISI 1018 mild steel, nickel, and Al<sub>2</sub>O<sub>3</sub> coatings, the application of these coatings to real-world vehicular and construction industry is still under research.

According to the literature, further study is needed to compare the effects of nickel and Al<sub>2</sub>O<sub>3</sub> on corrosion, wear, and mechanical performance. Based on the aforementioned information, the goal of the current study is to evaluate the physical, morphology, tribological, and corrosive efficiency of Ni-Nano Al<sub>2</sub>O<sub>3</sub> covered AISI 1018 mild steel produced using the reverse pulse electro deposition method. The proposed samples coated with the optimum percentages of nickel and Al<sub>2</sub>O<sub>3</sub> is preferable for the structural components of aircraft structures, armors of the defense vehicles and medical grade equipment's.

## Experimental Procedure

### Samplepreparations process

The elemental make-up of the base metal, AISI 1018 mild steel, provided by Bharath Metals, Chennai, is shown in Table 1. The delivery of Ni and Nano-Al<sub>2</sub>O<sub>3</sub> particles, with an average particle size of 45 nm, was made by Nanoshell in India. Mild steel served as the cathode for the pulse electrodeposition procedure, while a Ni plate of 100 mm × 30 mm × 10 mm served as the anode. Prior to the procedure, base materials must be cleared of contaminants. The plates were polished with 1800 grade SiC sheets before being submerged in acetone that had been ultrasonically cleaned for 15 minutes. Substrates were washed with distilled water at room temperature after the aforementioned procedure. Table 2, Fig. 1 shows the prepared samples.

Prior to the Ni- Al<sub>2</sub>O<sub>3</sub> electro deposition, the quantitative chemical and plain water were used to create the Ni- Al<sub>2</sub>O<sub>3</sub> electrochemical deposition liquid. Following the suspension optimizer 16-hour stirring period, the Al<sub>2</sub>O<sub>3</sub> nanoparticles (purity > 95%, spherical particle shape, concentration 10 g<sup>-1</sup>) were distributed in the electrolyte using sodium dodecyl sulphate. Under

**Table 2.** Watts bath formulations of Ni-Nano Al<sub>2</sub>O<sub>3</sub> coating.

S. No	Electroplating bath composition	Values
1	pH Value	4
2	Temperature (°C)	50 ± 2
3	Nickel Sulfate (NiSO <sub>2</sub> )	99 g/l
4	Boric Acid (H <sub>3</sub> BO <sub>3</sub> )	12 g/l
5	Sodium dodecyl sulfate (NaC <sub>12</sub> H <sub>25</sub> SO <sub>4</sub> )	0.4 g/l
6	Nickel Chloride (NiCl <sub>2</sub> )	15 g/l
7	Aluminium Oxide (Al <sub>2</sub> O <sub>3</sub> )	0.5-3 g/l

**Table 1.** Chemical composition of AISI 1018.

C	Mn	Si	S	P	Cr	Ni	N	Fe
0.08	2.00	0.75	0.03	0.045	19	8.75	0.10	69.245



**Figure 1.** (a) Ni- Al<sub>2</sub>O<sub>3</sub> uncoated sample, (b) Ni- Al<sub>2</sub>O<sub>3</sub> Coated samples.

**Table 3.** Electro deposition parameters.

S. No	Deposition parameters	Values
1	Anodic current density (ACD) (A cm <sup>-2</sup> )	0.04
2	Anodic current time (ACT) (s)	0.1
3	Cathodic current time (CCT) (s)	0.01
4	Cathodic current density (CCD) (A cm <sup>-2</sup> )	1.0
5	Relaxation time (RT) (s)	0.1
6	Temperature (°C)	50

the pulse reverse current (PRC) approach, Ni- Al<sub>2</sub>O<sub>3</sub> ceramic coatings were successfully deposited from a nickel Watts type bath. A plating cell holding 250 ml of solution having pH set at 4 and maintained at a temperature (50 °C), temperature and humidity regulated by a thermal mixer, was mixed with the prepped Al<sub>2</sub>O<sub>3</sub>. Similarly electro deposition parameters set for the proposed coatings were reported in Table 3.

By employing Cu- $\alpha$  radiation source and X-ray diffraction (MiniFlex), the morphology of the Ni-Al<sub>2</sub>O<sub>3</sub> composite was explored. SEM (version 4.0 Beta, Carl Zeiss, Germany) was used to analyze the surface morphology of coatings. Crystalline materials are characterized by X-Ray Diffraction analysis (XRD). Phase identification is often done using X-ray diffraction patterns, which are specific to the periodic atomic configurations in a material. In a diffractometer, incoming X-rays are reflected (diffracted) from the sample's lattice planes at certain angles, producing diffraction peaks indicative of the crystal structure of sample. Phase, crystal structure, preferred orientation,

average grain size, crystallinity, strain and crystallite size. All these information that may be gleaned from the diffraction patterns. Using a Vickers micro hardness Shimadzu tester with a 100 g pressure applied for 15 s, the micro hardness of the coatings was ascertained. The average of 5 individual measurements makes up the quoted hardness. Tests for corrosion caused by salt spray and dry sliding wear patterns (ASTM G-99-95a) of the samples were also looked at and documented.

In order to conduct the wear experiment, a pin-on-disc is employed. Before testing, the wear track, alloy, and composite specimens are carefully cleaned with acetone. The next step is to weigh each specimen using a digital balance with an accuracy of 0.001 gramme. The specimen is then put on the tribometer's pin holder and prepared for the wear test. The samples were used to create specimens with 12 mm diameters and 15 mm lengths, which were subsequently machined and polished. The sample is kept pushed against a revolving EN32 steel disc (hardness of 65HRC) throughout the test by applying pressure. By adopting a salt spray approach with NaCl solution and immersed corrosive tests with NaCl to mimic natural corrosion, the corrosion experiments were carried out in compliance with ASTM B117 criteria for corrosion testing. The specifications of the corrosion test method are shown in Table 4.

Six unique samples were prepared by varying nano Al<sub>2</sub>O<sub>3</sub> weight percentages from 0.5-3.0 and the results were compared with the uncoated samples. After coating, the efficiency of the suggested coating method and nanofillers on AISI 1018 mild steel was examined

**Table 4.** Details of salt spray corrosion testing parameters.

Particulars	Testing Parameters
Humidity	98% as measured by hygrometer
Temperature	33 to 35 Degrees centigrade
Pressure of air - atomizing regulator	2 to 3 bar continuously by pressure
Composition of the salt solution For 1 litre of solution	3.5% of NaCl, 1% of Magnesium chloride, De-ionized water 94%
PH of the buffer solution	Maintained at 7.5
Measurement of pH	Once in 8 hours
Type of loading of specimens in hanger	Tied with plastic wire and hung in

**Table 5.** Composition of the coated samples.

Sample Code	Electroplating bath composition and Al <sub>2</sub> O <sub>3</sub> Percentages
Neat	(NiSO <sub>2</sub> ) + (H <sub>3</sub> BO <sub>3</sub> ) + (NaC <sub>12</sub> H <sub>25</sub> SO <sub>4</sub> ) + (NiCl <sub>2</sub> ) + 0 %Al <sub>2</sub> O <sub>3</sub>
HMSAL1	(NiSO <sub>2</sub> ) + (H <sub>3</sub> BO <sub>3</sub> ) + (NaC <sub>12</sub> H <sub>25</sub> SO <sub>4</sub> ) + (NiCl <sub>2</sub> ) + 0.5 %Al <sub>2</sub> O <sub>3</sub>
HMSAL2	(NiSO <sub>2</sub> ) + (H <sub>3</sub> BO <sub>3</sub> ) + (NaC <sub>12</sub> H <sub>25</sub> SO <sub>4</sub> ) + (NiCl <sub>2</sub> ) + 1 %Al <sub>2</sub> O <sub>3</sub>
HMSAL3	(NiSO <sub>2</sub> ) + (H <sub>3</sub> BO <sub>3</sub> ) + (NaC <sub>12</sub> H <sub>25</sub> SO <sub>4</sub> ) + (NiCl <sub>2</sub> ) + 1.5 %Al <sub>2</sub> O <sub>3</sub>
HMSAL4	(NiSO <sub>2</sub> ) + (H <sub>3</sub> BO <sub>3</sub> ) + (NaC <sub>12</sub> H <sub>25</sub> SO <sub>4</sub> ) + (NiCl <sub>2</sub> ) + 2 %Al <sub>2</sub> O <sub>3</sub>
HMSAL5	(NiSO <sub>2</sub> ) + (H <sub>3</sub> BO <sub>3</sub> ) + (NaC <sub>12</sub> H <sub>25</sub> SO <sub>4</sub> ) + (NiCl <sub>2</sub> ) + 2.5 %Al <sub>2</sub> O <sub>3</sub>
HMSAL6	(NiSO <sub>2</sub> ) + (H <sub>3</sub> BO <sub>3</sub> ) + (NaC <sub>12</sub> H <sub>25</sub> SO <sub>4</sub> ) + (NiCl <sub>2</sub> ) + 3 %Al <sub>2</sub> O <sub>3</sub>

\*HMSAL – Hybrid Aluminium Oxide Coated Mild Steel

using X-ray diffraction, Scanning Electron Microscopy research, hardness, corrosion, and wear testing, and the findings were provided for the debate. The chemistry of samples coated with various pulse reverse settings and Al<sub>2</sub>O<sub>3</sub> percentages is clearly seen in Table 5. The following noteworthy insights are found via careful observation.

## Result and Discussion

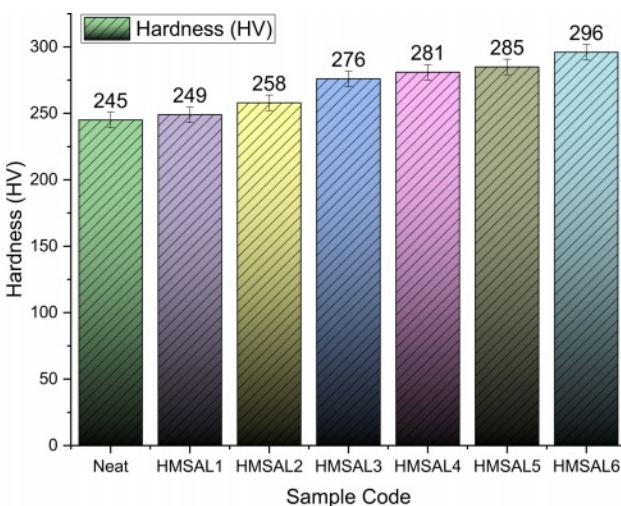
### Micro hardness test results

In order to utilize the plated specimens for the suggested purposes, the micro hardness of the samples has to be assessed. The employed reverse pulse electro deposition parameter's micro hardness level appears to be strongly impacted by an Al<sub>2</sub>O<sub>3</sub> % as well.

It was observed that uncoated samples penetrated more when compared to the different hybrid coated samples. This phenomenon is due to the higher surface toughness of the Al<sub>2</sub>O<sub>3</sub> coatings. To understand the penetration behavior of the samples, hardness values were depicted in the Fig. 2 along with the hardness of uncoated mild steel samples. The hardness of the samples ranges from 249 HV to 296 HV, and it can be

seen from the figure that there are very little variances in the hardness values due to the tiny variations in Al<sub>2</sub>O<sub>3</sub> percentages.

Neat samples exhibit 245 HV at 0.5 N load whereas 0.5, 1, 1.5, 2, 2.5 and 3 wt. % Al<sub>2</sub>O<sub>3</sub> filled composites exhibit 249 HV, 258 HV, 276 HV, 281 HV, 285 HV and 296 HV. A maximum indentation depth of 0.283 μm was observed during the indentations. During the indentations, a good amount depth of 0.226 μm was noted. Additionally, the hardness of the substrates and that of the tidy samples were contrasted. Over 20% tougher than uncoated samples, the HMSAL6 surface. Due to the significant difference in hardness between the surface and the neat samples, the ploughing effect of the neat samples should cause the surface to become worn down during the application of the substrate's sliding coating. Additionally, the small irregularities in the electrodeposited layers of Ni-Al<sub>2</sub>O<sub>3</sub> may be the cause of the significant confidence interval (0.32) in the hardness of the Al<sub>2</sub>O<sub>3</sub> coating relative to the neat sample. These findings suggest that Ni-Al<sub>2</sub>O<sub>3</sub> was a viable interfacial material for altering the surface energy of the Ni-Al<sub>2</sub>O<sub>3</sub> electrodeposit with improved structural uniformity.

**Fig. 2.** Hardness comparison of the various test samples.

### Salt spray corrosion test

The saltwater spray rust test is frequently used in labs to assess a material's ability to corrode since it is an accelerated type of corrosion test that results in deterioration in the part of the sample exposed to the corrosive media. A NaCl solution with a pH of 7.5-8 (3.5 percent sodium chloride, 1% magnesium chloride, and 94% de-ionized water) was used for the salt spray test. The rate of rust was monitored for 24 hours.

According to ASTM B117 standards, the weight loss for each sample subjected to the submerge experiment was evaluated [34]. According to ASTM protocols, the cumulative corrosion rate for every sample was estimated using data from weight loss measurements. Fig. 3 and 4 depict the weight loss and rust trends for the hybridised test specimens made from the NaCl solution sprayed specimens. The NaCl solution is tested for spray corrosion over a period of 12 to 96 hours, with

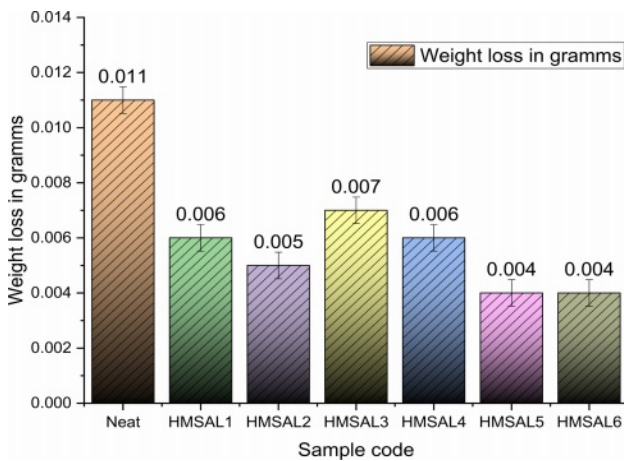


Fig. 3. Weight loss of the various test samples.

an 8-hour break in between experiments. Furthermore, the specimens with a 3 percent Al<sub>2</sub>O<sub>3</sub> coating showed improved corrosion resistance as compared to other Ni-Al<sub>2</sub>O<sub>3</sub> reinforcement percent's. Because grain boundary precipitation occurs over a longer period of time, persistent anodic stream stopping is associated with improved abrasion resistance [30]. Due to the prolonged exposure of salt water on the metal surface the salt layers sediments and it causes severe corrosion on the metal surface over a time. This corrosion improves the metal erosion rate and reduces the weight of matrix material.

In spray corrosion testing, the weight reduction of recommended mild steel-Al<sub>2</sub>O<sub>3</sub> coatings with varying Al<sub>2</sub>O<sub>3</sub> percent's did not follow a predictable pattern. Identical to Fig. 3, Fig. 4 shows the corrosion rate discovered during salt spray experiments on several hybrid samples. It was interesting to notice that the HMSAL6 and Neat samples showed the lowest corrosion rate of 0.152 mils/year and 1.421 mils/year, respectively. Additionally, it was demonstrated that by extending the time that Mild steel samples coated with

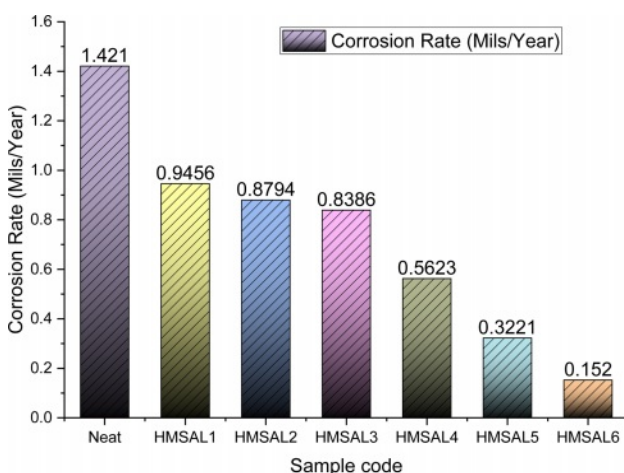


Fig. 4. Corrosion rate of the various test samples.

varying percentages of Ni-Al<sub>2</sub>O<sub>3</sub> were in interaction with the solution, considerable corrosion behaviour was obtained [31]. In this proposed experiment there is a reasonable corrosion rate were seen in all the samples whereas neat samples exhibits higher weight loss and corrosion rate.

### Dry sliding wear behaviour of hybrid samples

The estimation of the wear parameters of hybridized samples depends critically on the resistance between the suggested material and the matching tribo (E31) region. Based on the wear rate and coefficient friction values, friction is typically the final consequence of asperity distortion, ploughing, and attraction [26]. For the investigation in this suggested study, the wear variables listed below were taken from the publications [21-26]. For the conversations, the following information was provided: load of 5 N, sliding speed of 0.5 m/sec, sliding distance of 200 m, and observed outcomes. Figs. 5 and 6 show the samples' observed COF and wear rate. A lower COF indicates more abrasion resistance.

According to Fig. 5, the co-efficient of friction has a fluctuating value, and among all the specimens, HMSAL6 has the lowest COF (0.326). The higher solubility of fillers and matrix material is to blame for this phenomena. In the trials carried out by Bowkett [28], a similar pattern of findings was seen. Fig. 6 displays the wear rates for different combinations, and it is clearly obvious that HMSAL6 reports a reduced wear rate of around 402.185 Micron whereas HMSAL1, HMSAL2, HMSAL3, HMSAL4, HMSAL5 and Neat samples exhibits wear rates of 793.215, 602.258, 629.154, and 552.65, 478.65 and 405.658 Micron, respectively. Compared to other configurations, HMSAL6 has a wear resistance that is over 40% greater. Wear behaviour of the samples mostly depends on the nano particles reinforced in the matrix. In this way the

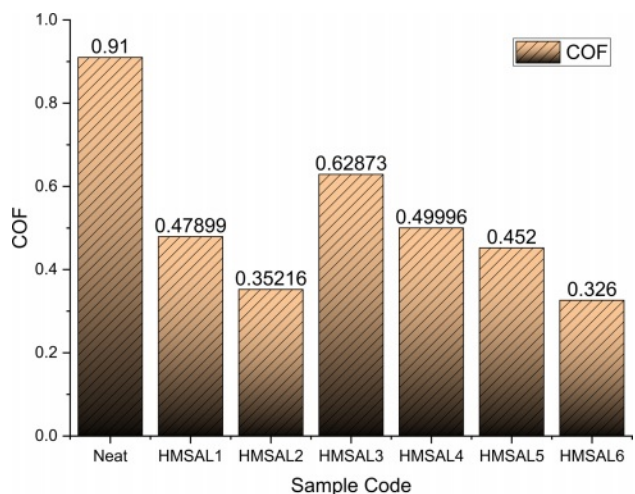


Fig. 5. COF comparisons of various test samples.

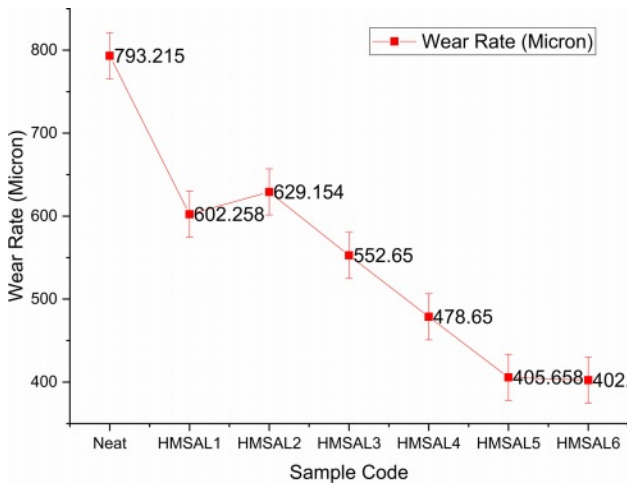


Fig. 6. Wear rate comparisons of various test samples.

proposed samples contains alumina and Ni coating on the surface which strictly resists the metal wear significantly.

**SEM analysis of samples before and after corrosion**

Figure 7 displays images of the hybridized samples acquired using scanning electron microscopy at various magnifications up to 1500X. The neat and HMSAL1 samples are shown in Figs. 7(A) and (B), correspondingly. Al<sub>2</sub>O<sub>3</sub> mixtures of 2.5 and 3 weight percent are shown

in Figs. 7(C) and (D), respectively. The images unequivocally demonstrate how the tiny elements will disperse over the grid. Higher magnification images of the coated surface layer are shown in Fig. 7(C) and (D). Characterization research revealed that HMSAL6 (3 wt. % Al<sub>2</sub>O<sub>3</sub>) yields better outcomes, which was revealed based on those findings. Fig. 8 shows the XRD data that were taken from every hybrid composite in order to validate the research and materials.

Rust of the cementitious material has a number of typical impacts on its crystallites and causes additional structural loss, which considerably reduces the product's durability and longevity. The rusted sides of the components were retrieved or examined for their microstructural characteristics by field emission scanning electron microscopy at magnifications ratios. After the electron beam spitting process had solidified at magnifications, SEM images were taken in a variety of settings (Up to 2000X).

During the corrosive interface examination, micro-grooves, ploughing, and tiny abrasion were found. Hard Al<sub>2</sub>O<sub>3</sub> particles are added to composite samples to increase their hardness, which are the principal causes of corrosion, surface cracks, and debonding. In Ni-Al<sub>2</sub>O<sub>3</sub> coated samples, surface defects such coating peel out, porosity, and adhesion debris were discovered. Similar findings could be observed in the literature [24, 26].

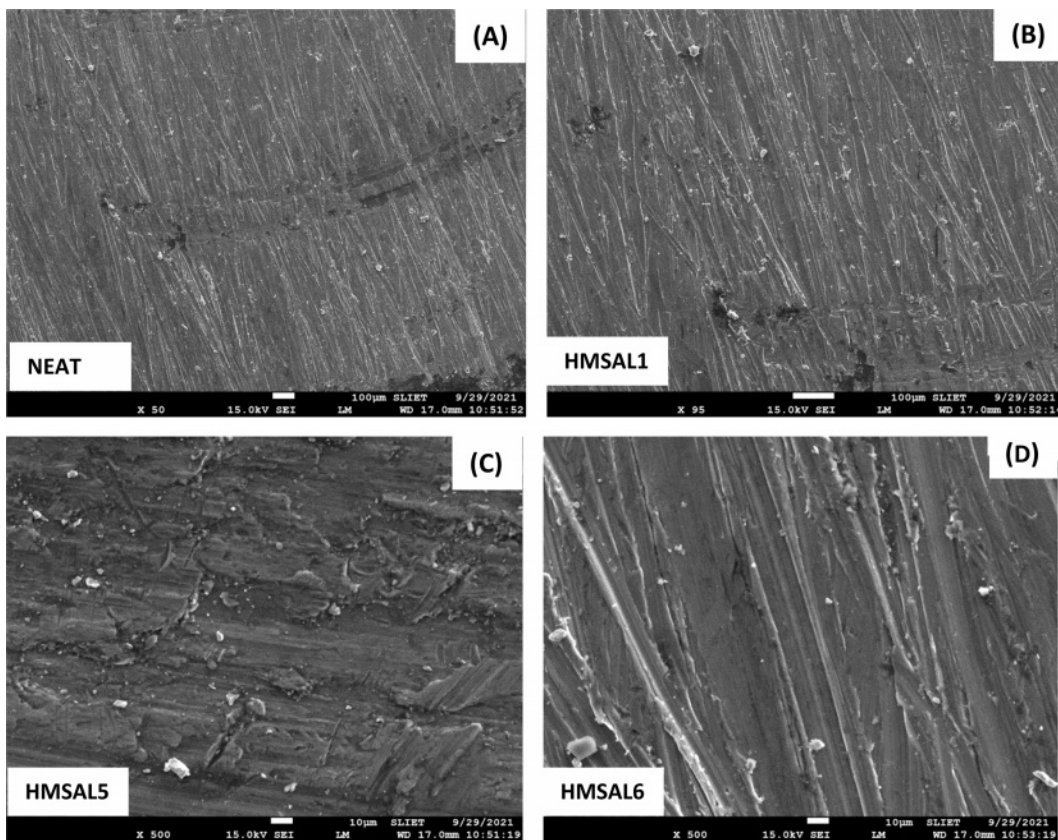
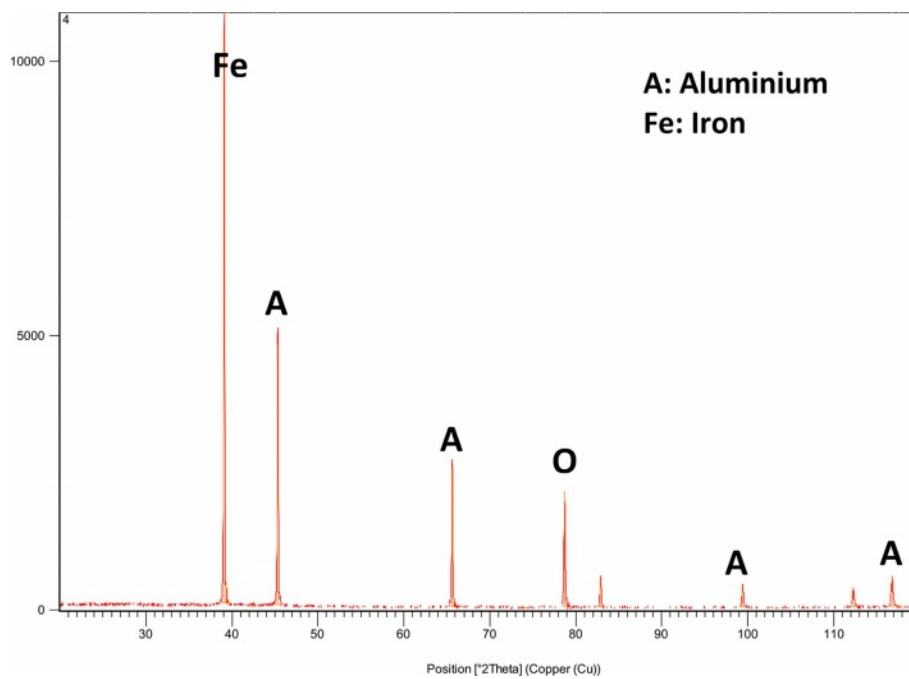


Fig. 7. Scanning electron microscopic images of samples before corrosion.



**Fig. 8.** Intensity vs.  $2\theta$  chart of HMSAL6 sample.

Following a salt spray corrosion test, the HMSAL6 arrangement is seen in SEM microphotographs in Fig. 9. The damaged parts may be seen as minute cracks on SEM images after submitting the material to a salt spray corrosion test. Following spray corrosion

testing, Fig. 9 displays SEM microphotographs of composite materials with varying  $Al_2O_3$  percents (C and D). The damaged regions may be seen as minute cracks and pitting on SEM images after the material has undergone an immersion corrosion test.

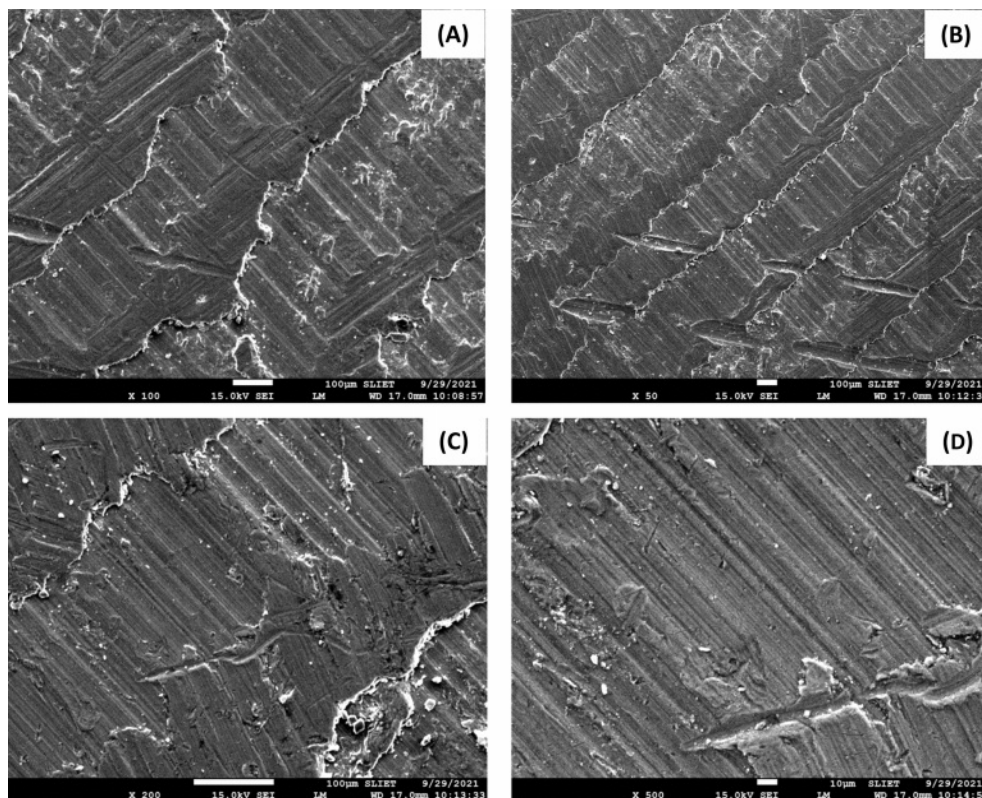


**Fig. 9.** Scanning electron microscopic images of corroded surface.

## Conclusion

The research project involves the construction of Ni-Al<sub>2</sub>O<sub>3</sub> plated mild steel specimens using a reverse pulse deposition technique, as well as an analysis of the material's hardness, corrosion, wear, and morphology both before and after corrosion. According to the experiment's findings, the 3 weight percent Al<sub>2</sub>O<sub>3</sub> plated HMSAL6 samples had 296 HV hardness, which is over 25% more than the plain samples. Similar to this, research on corrosion and wear show that increasing the proportion of Ni-Al<sub>2</sub>O<sub>3</sub> gradually improves the corrosion and wear characteristics by up to 25% and 40%, correspondingly. Increased resilience to salt spray corrosion and wear is demonstrated by HMSAL6. As a result, the geometry of the steel surface both before and after corrosion was examined, and it was found to have an equal distribution of Ni-Al<sub>2</sub>O<sub>3</sub> particles. The important results of this study effort might be applied in numerous industrial settings where wear and corrosion is a prominent concern because of the present need for nanocomposite coverings.

## References

1. U. Pandey, A.K. Singh, and C. Sharma, *Synth. Met.* 290 (2022) 117135.
2. F. Mahdi, M. Javanbakht, and S. Shahrokhian, *J. Energy Storage.* 46 (2022) 103802.
3. E. Rahali, M.M. Alves, L. El-Bassi, and L. Bousselmi, *Prog. Org. Coat.* 163 (2022) 106602.
4. S. Kumar, and A.K. Das. *Eng. Res. Express.* 4 (2022) 015034.
5. H. Wang, Y. Sun, Y. Qiao, and X. Du, *Opt. Laser Technol.* 142 (2021) 107209.
6. D.E. Raja, S.P. Singh, V. Rangarajan and M.C. Das, *J. Ceram. Process. Res.* 23[6] (2022) 926-933.
7. H. Fan, J. Jiang, Y. Zhao, S. Wang, and Z. Li, *Int. J. Mod. Phys. B* 34[27] (2020) 2050243.
8. M. Aliofkhaezrai, F.C. Walsh, G. Zangari, H. Kockar and M. Alper, *Appl. Surf. Sci. Adv.* 6 (2021) 100141.
9. Z. Mahidashti, M. Aliofkhaezrai, and N. Lotfi, *Trans. Indian Inst. Met. T.* 71 (2018) 257-295.
10. E. Natarajan, K. Markandan, K. Varadaraju, and Saravanakumar, *J. Compos. Sci.* 6[10] (2022) 310.
11. S. Kaliappan and Pravin P. Patil, *J. Nanomater.* 2022 (2022) 5465771.
12. A.R. Shahmoradi and M. Ranjbarghanei, *J. Mol. Liq.* 338 (2021) 116550.
13. W. Zhang, B. Nie, H.J. Li, Q. Li, C. Li, and Y.C. Wu, *Carbohydr. Polym.* 260 (2021) 117842.
14. E.X. Ricky, M. Mpelwa, and X. Xu, *J. Ind. Eng. Chem.* 101 (2021) 359-371.
15. M.P. Jahan, Y.S. Wong, and M. Rahman, *J. Mater. Process. Technol.* 209[8] (2009) 3956-3967.
16. C.C. Satheesh, J. Jayapriya, and P. Prabunathan, *J. Polym. Environ.* 30[4] (2022), 1528-1546.
17. Y. Sun, H. Wang, W. Liu, G. Song, and Q. Li, *Surf. Coat. Technol.* 368 (2019) 215-223.
18. S. Thapliya and D. Dwivedi, *J. Mater. Process. Technol.* 238 (2016) 30-38.
19. R. Girmurugan, J. Bensamraj, and S.J. Karthick, *Ceram. Process. Res.* 23[4] (2022) 553-557.
20. X. Feng, X. Cui, G. Jin, W. Zheng, Z. Cai, X. Wen, B. Lu, and J. Liu, *Surf. Coat. Technol.* 333 (2018) 104-114.
21. Q. Luo, Z. Wu, Z. Qin, L. Liu, and W. Hu, *Surf. Coat. Technol.* 309 (2017) 106-113.
22. W. Qian, Y. Hua, R. Chen, P. Xu, and J. Yang, *Mater. Lett.* 268 (2020) 127570.
23. M. Dehestani, G.R. Khayati, and S. Sharafi, *Meas.* (2021) 109423.
24. X. Chu, L. Gan, S. Ren, and J. Wang, *Ceram. Int.* 46[6] (2020) 8413-8419.
25. C.R. Raghavendra, *J. Adhes. Sci. Technol.* 36[21] (2021) 2297-2312.
26. Z. Lin, W. Zhang, L. Xu, Y. Xue, and W. Li, *Mater. Chem. Phys.* 277 (2022) 125503.
27. H. Huang, S. Li, B. Chen, Y. Wang, Z. Shen, and M. Qiu, *J. Colloid Interface Sci.* 627 (2022) 705-715.
28. M. Bowkett, M.H. Nazir, M.M. Hussain, and Z.A. Khan, *Appl. Sci.* 12[9] (2022), 4283.
29. M. Shahida, R.A. Malika, H. Alrobeib, and J. Kimc, *J. Ceram. Process. Res.* 22[2] (2021) 149-157.
30. J.S. ShathishKumar and A. Jegan, *Int. J. Electrochem.* 16[4] 2021.
31. X. Dai, K. Xu, Z. Zhang, L. Zhang, Y. Wu, and H. Zhu, *J. Electroanal. Chem.* 904 (2022) 115855.
32. D.-S. Lee, H. Kong, and S.-J. Le, *J. Ceram. Process. Res.* 23[2] (2022) 137-144.
33. P. Mandal and S.C. Mondal, *Mach. Sci.* 25[3] (2021) 422-437.
34. E. Natarajan and L. Freitas, *Def. Technol.* 19 (2023) 1-11.
35. R. Sasikumar and E. Natarajan, *Mater. Res. Express* 4[8] (2022) 045310.